IL NUOVO CIMENTO **41 C** (2018) 123
DOI 10.1393/ncc/i2018-18123-7

COMMUNICATIONS: SIF Congress 2017

An optimisation procedure for pulse shape discrimination algorithms tailored for hand-held nuclear security instruments

L. MALINVERNO(*)

Università degli Studi dell' Insubria, Dipartimento di Scienza ed Alta Tecnologia - Via Valleggio 11, 22100 Como, Italy

received 27 January 2018

Summary. — Nuclear security has strict requirements on hand-held instrumentation. The detectors have to be neutron sensitive, capable to discriminate between neutrons and gammas, possibly providing the gamma emitter identification. The detecting unit has to be compact, low power consuming and integrated into systems to perform on-line data analysis and to assess the alarm level according to the international standards. This paper reports an optimization procedure for pulse shape discrimination algorithms developed for detectors based on neutron sensitive scintillators coupled to photo-sensors. As a specific case study, data collected for a volume of EJ 299-34 material coupled to Silicon Photomultipliers were analysed.

1. – Introduction

In the last decades an increasing volume of illicit trafficking of radioactive sources has been observed representing a threat to national and international security [1]. The threat arises from terroristic-end purposes as well as from the unauthorised use of radioactive materials for industrial applications [2]. An additional hazard is represented by the so-called *orphan sources*, namely radioactive material illegally disposed of.

The strict enforcement of border controls and the availability of instruments for first respondents and police units is considered a priority at governmental and international level. Nowadays different policing instruments exist to face that hazard. The Radiation Portal Monitors (RPM) are a class of devices intended for a preliminary scan of trucks or containers at borders or at the entrance of reprocessing facilities where contaminated radioactive waste can be identified. If a cargo is tagged as suspicious, portable devices can be used to assess the risk level accordingly to the International Atomic Enery Agency (IAEA) guidelines [3, 4].

(*) E-mail: l.malinverno1@uninsubria.it

Fig. 1. – The experimental set-up based on the EJ 299-34 coupled with the Hamamatsu s13361-3050AE-04 MPPC Array. The Hamamatsu C11204-01 supplies for the bias voltage.

Moreover the counter-actions against non-state actors aiming to build Radiological Dispersal Devices (RDD), a threat outlined by the IAEA, may benefit from a smart grid of hand-held devices supplied to police patrols and distributed on the public transportation network, as, for example, the D3S® produced by Kromek™ [5].

Cost and performance optimization is steering the development of a new class of hand-held detectors employing solid state scintillation materials coupled to Silicon Photomultipliers (SiPM) and is exploited by a number of research institutions and companies in the world [6-11]. The reported activity is part of this research stream. It focuses on the comparison of Pulse Shape Discrimination algorithms compliant with real-time processing, and discusses procedures for the optimization of these algorithms.

2. – Materials and methods

The detecting unit (fig. 1) consists in a bar of EJ 299-34 plastic scintillator coupled to an array of 16 SiPMs. Each SiPM in the array has dimension of $3 \times 3\,\mathrm{mm}^2$ with the main characteristics reported in table I. A custom front-end electronics module supplies the bias to the sensor, sums-up the output from the SiPM array elements and amplifies the total signal, feeding a waveform digitizer [12]. The output from the array has been digitised with a CAEN DT5720 module, sampling the signal at 250 MS/s with 12 bit resolution. The reported analyses have been performed off-line on samples of recorded events.

The EJ 299-34 is a plastic scintillator produced by Eljen technologies sensitive to fast neutrons and γs, with pulse shape discrimination capability [13]. The temporal development of the light generated by a γ interaction is a sum of 3 decaying exponential curves with decay times of 15, 35 and 270 ns; the neutron interaction, *i.e.* scattering with hydrogen nuclei, produces light with decay time of 15, 50 and 450 ns as reported on the data sheet. The light yield is 7000 photons per MeV. The scintillator used for the present work has dimensions of $10 \times 10 \times 50\,\mathrm{mm}^3$ and was wrapped with Teflon tape to improve the light collection.

Four different discrimination algorithms were compared; the algorithms were selected to require low computational power aiming for, at a later stage, a real-time FPGA or DSP module implementation.

TABLE I. – *Main characteristics of the SiPM array used for this analysis.*

Hamamatsu S13361-3050AE - 04		
Number of SiPMs	16	–
Single SiPM size	3×3	mm^2
Pixel pitch	50	μm
V_{BD}	50	V
V_{op}	$V_{BD} + 5$	V
Gain	$1.7 \cdot 10^6$	–
DCR	0.5	Mcps
Cross-talk	<5	%
PDE_{MAX}	40	%
Fill factor*	74	%
Dead area**	0.2	mm

* Fill Factor referred to a single SiPM.
** Dead area between two neighbouring SiPMs.

An exemplary illustration of the difference in the temporal development of the scintillation light emission by γs and neutrons is shown in fig. 2. The average signals arise from 150 events recorded by the system exposed to a ^{252}Cf source and selected in the energy interval between 1 and 1.5 MeV. The γ-neutron discrimination technique was selected from the best among the following algorithms.

The compared discrimination algorithms are defined as follows.

- *Constant Time:* the Constant Time (CT) algorithm discriminates on the basis of the value of the signal $S(t)$, at time t with respect to the onset, normalized to the

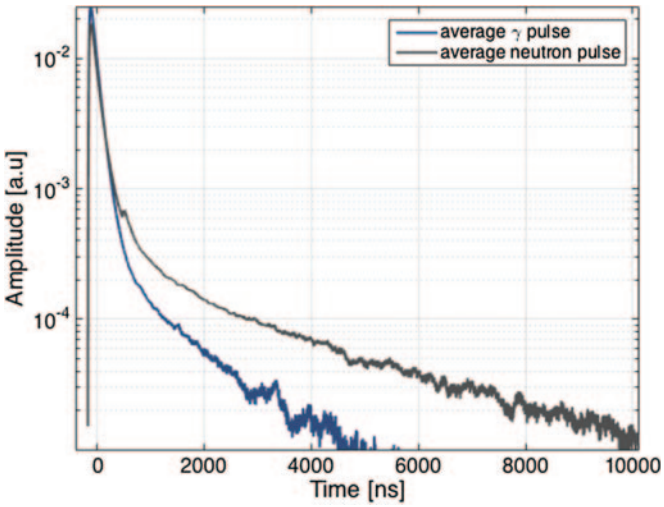

Fig. 2. – Average of 150 pulses from γ and neutron events, normalised to the area under the signals.

total signal area [14].

$$PSD = \frac{S(\bar{t}_{CT})}{\int S(t)\mathrm{d}t}, \tag{1}$$

where $\bar{t}_{CT}$ is the time lapse since the onset of the signal.

- *Pulse Gradient Analysis:* the Pulse Gradient Analysis (PGA) algorithm discriminates the pulses on the basis of the value of the signal $S(t)$, at time t with respect to the onset, normalised to the peak [15].

$$PSD = \frac{S(\bar{t}_{PGA})}{\max\{S(t)\}}, \tag{2}$$

where, as above, the $\bar{t}_{PGA}$ is the time lapse since the onset of the signal.

- *Charge comparison:* the Charge Comparison algorithm (CC) discriminates the pulses on the basis of the ratio between the integral of the signal tail and the total signal area [16].

$$PSD = \frac{\int_{t_{delay}}^{t_{int}} S(t)\mathrm{d}t}{\int S(t)\mathrm{d}t}, \tag{3}$$

where t_{delay} is the time lapse since the onset of the signal from where the integration window, that last t_{int}, starts.

- *Peak-Tail:* the Peak-Tail algorithm (PT), originally proposed by the author, normalises the signal to the peak value rather than the total area and considers the integral value in the tail.

$$PSD = \frac{\int_{t_{delay}}^{t_{int}} S(t)\mathrm{d}t}{\max(S(t))}, \tag{4}$$

where t_{delay} and t_{int} are defined as for the CC algorithm.

3. – Pulse Shape Discrimination Optimisation

3˙1. *Energy Calibration.* – The radionuclides of interest emit γs with energies that predominantly interact through the Compton Scattering as the EJ 299-34 has low atomic number [17]. To provide a reliable energy calibration, a procedure avoiding the usual Monte Carlo simulation techniques is proposed [18]. The calibration procedure exploits the use of the maximum deposited energy (eq. (5)) for the Compton scattering interaction when the Compton edge is fitted with a Gaussian error function.

$$E_{max} = \frac{2E_\gamma^2}{2E_\gamma + m_e c^2} \tag{5}$$

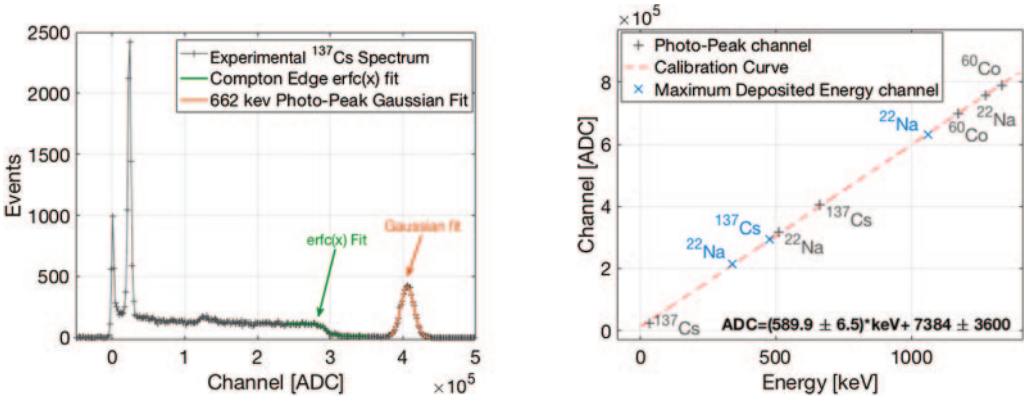

Fig. 3. – On the left hand side the ^{137}Cs spectrum obtained with the CsI crystal is reported. On the right hand side the calibration curve calculated with the use of the photo-peak position (grey points) is shown. The maximum deposited energy points (blue points) hold to the same calibration curve.

Since the analytical form of the Compton Edge presents a sharp edge at the maximum deposited energy value, it has been modelled as a stepwise function ($\Theta(x)$). The stochastic terms, assumed to be Gaussian, convoluted with the $\Theta(x)$ give a complementary Gaussian error function, as shown in eq. (6).

$$\Theta(\eta) \otimes G(\eta) = \int_{-\infty}^{+\infty} \Theta(\eta - \tau) G(\tau) \mathrm{d}\tau, \tag{6a}$$

$$\int_{-\infty}^{\eta} \Theta(\eta - \tau) G(\tau) \mathrm{d}\tau = 0, \tag{6b}$$

$$\Theta(\eta) \otimes G(\eta) = \int_{\eta}^{\infty} G(\tau) \mathrm{d}\tau = \int_{\eta}^{\infty} e^{-\eta^2} \mathrm{d}\eta = \mathrm{erfc}(\eta), \tag{6c}$$

when η is written as in eq. (7), x_0 results to be the ADC channel corresponding to the maximum deposited energy.

$$\eta = \frac{x - x_0}{\sigma\sqrt{2}}. \tag{7}$$

In order to verify the reliability of the Compton edge fit, the procedure was tested with a CsI ($10 \times 10 \times 15\,\mathrm{mm}^3$) crystal, for which both the Compton scattering and the photo-peak absorption interaction have non negligible cross sections. Along with the calibration points obtained from the photo-peak energy, based on a Gaussian fit (orange line in fig. 3), the channels corresponding to the maximum deposited energy were obtained after the erfc(x) fit (green line in fig. 3) as shown in fig. 3. The R^2 for the photo-peak calibration points is 0.9999. When the maximum deposited energy channels are considered along with the photo-peak calibration points the R^2 decrease to 0.9997. The good agreement between the maximum deposited energy points and the calibration curve validates the procedure.

In fig. 4 the Compton edge fit for the ^{137}Cs spectrum obtained with the EJ 299-34 is reported along with the calibration curve for this plastic scintillator. The ^{60}Co point in

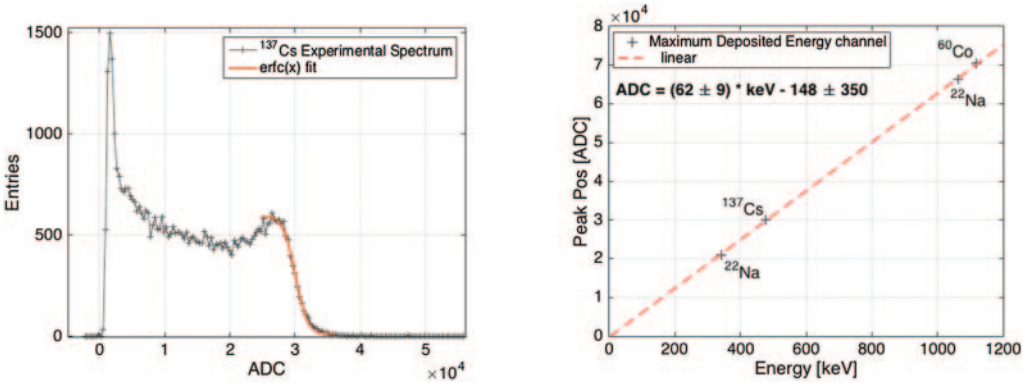

Fig. 4. – On the left hand side the spectrum of the Compton edge of a ^{137}Cs source collected with the EJ 299-34. On the right hand side the calibration curve is reported.

fig. 4 refers to the average energy of the two maximum deposited energy related to the 1.3 MeV and 1.1 MeV γs.

3˙2. *Optimisation procedure.* – The optimisation procedure involves the selection of the parameters that maximize the Figure of Merit (FOM) of the neutron-γ discrimination. The FOM is defined as follows:

$$FOM = \frac{|\overline{PSD_\gamma} - \overline{PSD_n}|}{FWHM_\gamma + FWHM_n}, \tag{8}$$

where $\overline{PSD_i}$ is the mean value of the pulse shape discrimination variable distribution in a given energy window and $FWHM_i$ was calculated as $2.355 \cdot \sigma$, since the distribution can be considered to be Gaussian shaped. This assumption is supported by the value of the $\chi^2/d.o.f.$ of the Gaussian fit in fig. 6: 1.007 for the γs distribution and 1.076 for the neutrons ones. A figure of merit in excess of ~ 1.3 stands for two distributions with a misidentification probability below 0.3%, while a FOM of 2 represents a misidentification probability of the order of 10^{-4}.

The FOM was calculated in the energy window 1–1.5 MeV with a scan over a set of parameters in order to find the parameters that maximise the FOM. The output of the optimisation scan for the PT and the CC algorithms is shown in fig. 5; the value of FOM is reported accordingly to the color legend, where X and Y axes are the value of the parameters t_{delay} and t_{int} corresponding to each FOM.

Figure 5 also points out that the PT algorithm presents a wider set of parameters that guarantees a good discrimination, accounting for its stability. The stability is quantified with the evaluation of the area in the parameters space where the FOM is above 2; this area exceed $4\,\mu$ s^2 for the PT algorithm and is about $2.15\,\mu$s^2 for the CC algorithm. The PT algorithm applied using $t_{delay} = 160$ ns and $t_{int} = 6400$ ns returns PSD values in function of energy as plotted in fig. 6. Along with the ^{252}Cf source results for the ^{60}Co and for the ^{137}Cs were also plotted. The distribution of the PSD in the energy range 1–1.5 MeV is reported in fig. 6 where the FOM of 2.49 ± 0.02 was calculated on the ^{252}Cf data.

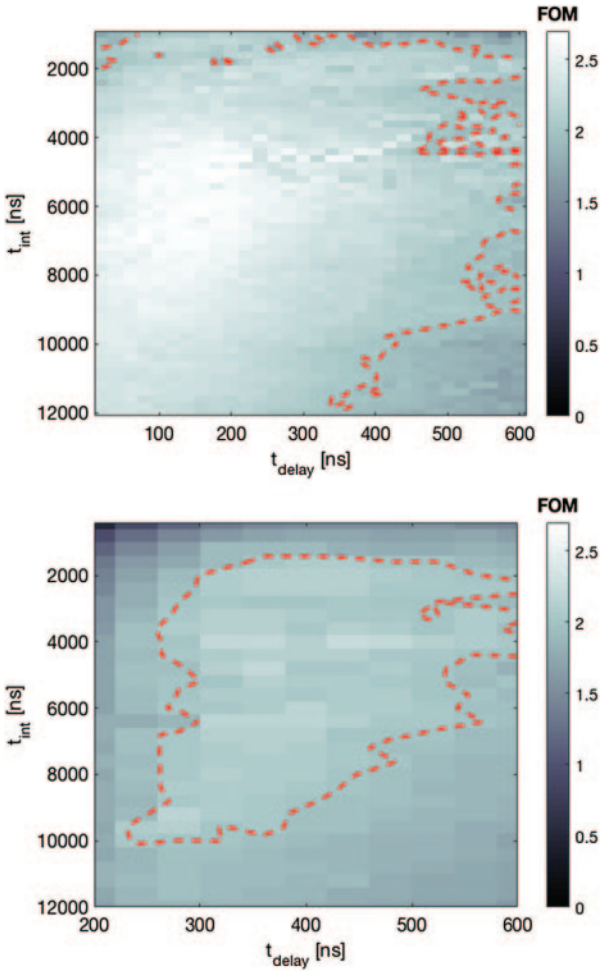

Fig. 5. – The top figure reports the output for the optimisation procedure applied to the PT algorithm, while the bottom one reports the result for the CC algorithm. The area in the parameters space where FOM is > 2 (red dashed line) is $\approx 4\,\mu s^2$ for the PT and $\approx 2.15\,\mu s^2$ for the CC.

The comparison of the algorithms by means of FOM in different energy windows and the minimum energy that presents a FOM exceeding 1.3 was carried out. The FOM comparison is reported in fig. 7. The minimum energy is reported in table II together with the FOM in the energy window 1–1.5 MeV.

In addition to the stability outlined by the optimisation analysis, the comparison of the PSD algorithms outlines that the Peak-Tail results in a better discrimination.

4. – Conclusions

A new method for the energy calibration of plastic scintillators has been proposed and validated, along with the comparison of different PSD algorithm after their optimisation. The Peak-Tail algorithm has been shown to give optimum performances both in the

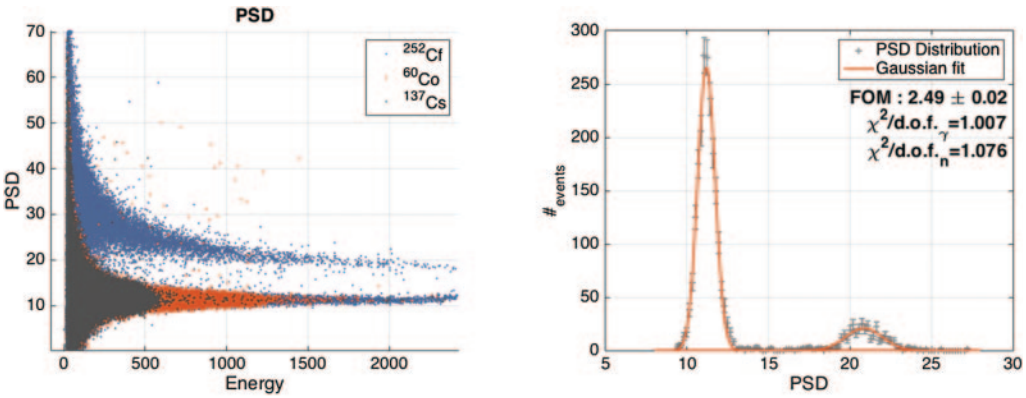

Fig. 6. – On the left hand side the distribution of the PSD is shown as a function of energy for the ^{252}Cf, the ^{60}Co and for the ^{137}Cs. Non linearity and saturation effects, due to the non linear region of the amplifier, occurs for energy greater than 2.5 MeV. On the right hand side the distribution of the PSD in the energy interval 1–1.5 MeV is shown with superimposed two Gaussian fits.

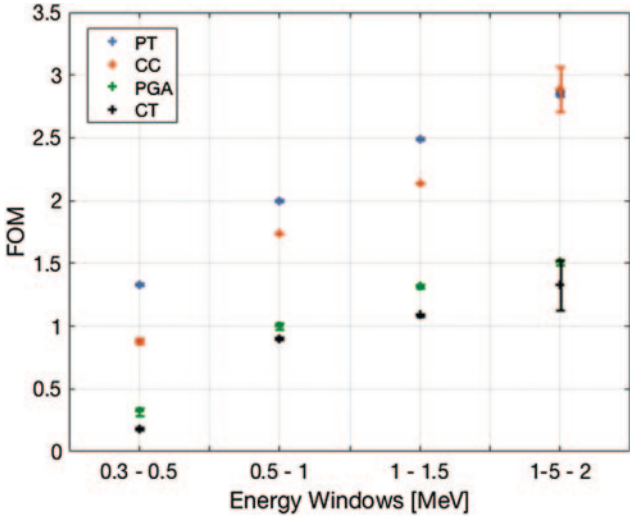

Fig. 7. – FOM in different energy windows for the compared algorithms.

TABLE II. – *FOM in the energy window 1–1.5 MeV and the minimum energy that allows for a FOM greater than 1.3*

	PT	CC	PGA	CT
FOM	2.49 ± 0.02	2.14 ± 0.01	1.32 ± 0.01	1.09 ± 0.02
min energy	200 keV	300 keV	1 MeV	1.5 MeV

discrimination power and stability. The PT algorithm also discriminates better at lower energy, making the discrimination possible down to 200 keV. Future studies will consider the applications of this algorithm to inorganic scintillators useful for thermal neutron detection and γ spectroscopy.

* * *

This research was performed under a collaborative research contract between Università dell'Insubria and KROMEK ltd, started on September 2017 with a three year duration. The author acknowledges the support by Massimo Caccia and Romualdo Santoro at the Dept. of Science and High Technology of Università dell'Insubria and Eward Mardsen and Ian Radley at KROMEK.

REFERENCES

[1] *Illicit trafficking of nuclear and other Radioactive Material, Tech. Rep.* (2012) available at: `http://www.vertic.org/media/assets/Publications/ITR_WEB.pdf`.
[2] IAEA, *Incident and trafficking database - ITDB* (2015) available at: `http://www-ns.iaea.org/security/itdb.asp`.
[3] IAEA, *Detection of Radioactive materials at borders* (2006) available at: `http://www-pub.iaea.org/MTCD/publications/PDF/te_1312_web.pdf`.
[4] IAEA, *Technical and Functional Specification for Border Monitoring Equipment, IAEA Nuclear Security Series, Technical Guidance* (IAEA, Vienna, Austria) 2008.
[5] Kromek, *Producer Data sheet*, available at `https://www.kromek.com/index.php/link-3/d3s# tab3-content`.
[6] Renker D., *Nucl. Instrum. Methods A* , **567** (2006) 48.
[7] Mesick K.E., arXiv:1520.01155v1 (2015).
[8] Brent S. Budden, in *IEEE Nuclear Science Symposium and Medical Imaging Conference Record (NSS/MIC)* (IEEE) 2012.
[9] Marc Lavi Ruch, Marek Flaska and Sara A Pozzi, *Nucl. Instrum. Methods A*, **793** (2015) 1.
[10] Preston R. M., *IEEE Trans. Nucl. Sci.*, **61** (2014) 4.
[11] Taggart M. P. *et al.*, *J. Phys.*, **763** (2007) 012007.
[12] Santoro R. *et al.*, *Qualification and performance of a neutron detector system with enhanced gamma discrimination, based on Silicon Photomultiplier arrays coupled to an EJ-299-34 scintillator IEEE-Explore*, in preparation (2018).
[13] Eljen Technology data sheet, available at `http://www.eljentechnology.com/products/plastic-scintillators/ej-299-33a-ej-299-34`.
[14] Sellin P. J., Jaffar G. and Jastaniah S. D., *Performance of digital algorithms for n - gamma pulse shape discrimination using a liquid scintillation detector*, in *2003 IEEE Nuclear Science Symposium Conference Record (IEEE Cat. No.03CH37515), Portland, OR, USA*, Vol. **2** (IEEE) 2003, pp. 1057–1060.
[15] Malcolm G. L. *et al.*, *IEEE Trans. Nucl. Sci.*, **57** (1999) 1682.
[16] Pozzi S. A. *et al.*, *Nucl. Instrum. Methods A*, **723** (2013) 19.
[17] Knoll G. F., in *Radiation Detection and Measurement* (John Wiley and Sons) 2016, pp. 49–50.
[18] HRISTOVA A. V. *et al.*, *Nucl. Instrum. Methods A* , **642** (2011) 70.